Available online at www.sciencedirect.com
ScienceDirect
Journal of Nuclear Materials 366 (2007) 407–416
journal of nuclear materials
www.elsevier.com/locate/jnucmat

# Alloying and microstructure stability in the high-temperature Mo–Si–B system

R. Sakidja *, J.H. Perepezko

*Department of Materials Science and Engineering, University of Wisconsin-Madison, 1509 University Avenue, Madison, WI 53706, USA*

**Abstract**

Multi-phase alloys in the Mo–Si–B system are identified as high-temperature structural materials due to their high melting points (above 2000 °C) and excellent oxidation resistance attributed to the self-healing characteristics of borosilica layer up to 1400 °C. In the current study, the effect of alloying additions to achieve a reduced weight density has been examined in terms of changes in the microstructure and phase stability. The critical factor underlying the microstructural changes is related to the influence of the alloying additions on the stability of the high melting temperature ternary-based $Mo_5SiB_2$ ($T_2$) borosilicide phase.


*PACS:* 81.05.Bx; 89.30.Gg; 64.75.+g

## 1. Introduction

The challenges of a high-temperature environment ($T > 1400$ °C) impose severe material performance constraints in terms of melting point, oxidation resistance and structural functionality. In this respect, the multi-phase microstructures developed from the Mo–Si–B system offer an attractive option [1,2]. The isothermal section at 1600 °C for the Mo-rich portion of the Mo–Si–B ternary system is shown in Fig. 1. Two-phase alloys based upon the coexistence of the high melting temperature (>2100 °C) and creep resistant ternary intermetallic $Mo_5SiB_2$ ($T_2$) with the Mo solid solution (BCC phase) allow for in situ toughening and a further possibility for strengthening through a precipitation of Mo within the $T_2$ phase [3]. Three-phase alloys comprised of Mo, $T_2$ and $Mo_3Si$ (A15) offer a promising balance of oxidation resistance and mechanical properties [4] due to the ductility of the Mo–BCC phase. The excellent oxidation resistance stems from the formation of a borosilica outer layer at low temperature and almost pure silica layer at high-temperature (due to the volatility of $B_2O_3$ above 1000 °C) on the surface during oxidation in air. Furthermore, there is a significant alloying substitution of molybdenum with other transition metals which potentially allows for significant modification in the materials properties.

One aspect of interest has been to lower the weight density of the overall Mo–Si–B alloys. In this respect, substitution of molybdenum with elements

* Corresponding author. Tel.: +1 608 263 2809.
*E-mail address:* sakidja@nucleus.msae.wisc.edu (R. Sakidja).

0022-3115/$ - see front matter © 2007 Elsevier B.V. All rights reserved.
doi:10.1016/j.jnucmat.2007.03.029

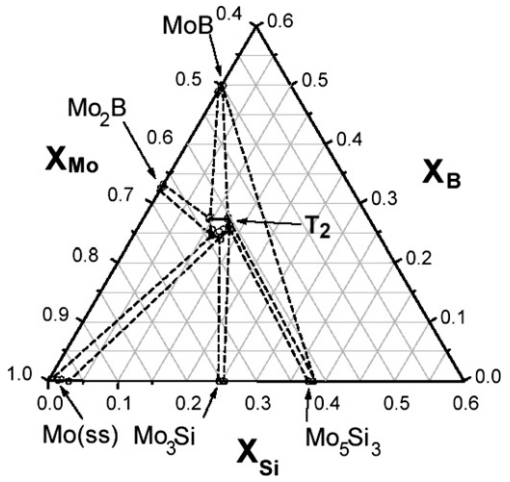


Fig. 1. The 1600 °C isothermal section of the Mo-rich portion of Mo–Si–B ternary system showing the existence of the BCC + $Mo_5SiB_2$ ($T_2$) + $Mo_3Si$ (A15) and $Mo_3Si + T_2 + Mo_5Si_3$ ($T_1$) three-phase phases [2].

such as titanium is an attractive option. As shown in Fig. 2, a Mo–20Si–10B (at.%) alloy which is comprised of a two-phase $Mo_3Si + T_2$, 50% substitution of Mo with Ti will enables a weight density drop from 9.5 to 7.6 g/cm$^3$. About 71% substitution of Mo by Ti yields Mo–Ti–Si–B alloys with a density less than 6.5 g/cm$^3$. Chromium substitution can also achieve a similar type of weight density reduction although to lesser extent. For example, Mo–10Si–20B (at.%) which consists of BCC Mo(ss) and $T_2$ phases has a weight density of about 9.7 g/cm$^3$. By substituting half of Mo with Cr, the density becomes 8.5 g/cm$^3$.

The important issue in this regard is how the alloying substitution would impact the critical properties such as the melting point and the oxidation resistance. The melting temperature and high-temperature properties in Mo–Si–B alloys are very much tied to the stability of the ternary-based intermetallic $T_2$ phase and the phase equilibrium that maintains the two-phase field of the ductile BCC phase with the $T_2$ phase.

The effect of Cr substitution on the microstructure and phase stability has been examined previously [2]. The current study focuses on elucidating the effect of the Ti alloying on the multi-phase microstructures, phase stability and the oxide structure formation. The Mo content in Mo–20Si–10B alloys was systematically substituted by Ti and the phase stability was examined following exposure to high-temperature annealing. Oxidation tests in air at temperatures between 700 and 1400 °C were conducted to evaluate the effect of the transition metal substitution on the oxide structures.

## 2. Experimental and analytical procedures

All Mo–Si–B and Mo–Ti–Si–B alloys with compositions of ($Mo_{100-X}$, $Ti_X$)–20Si–10B ($X = 0$–100)

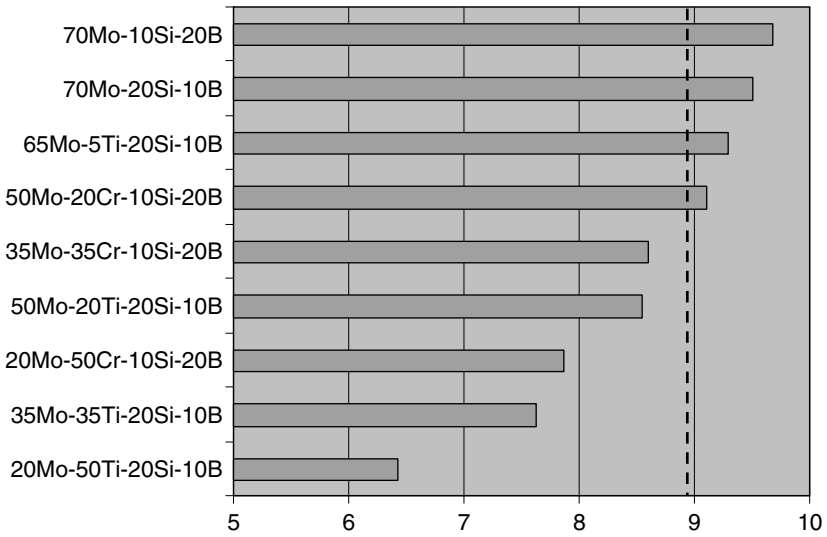


Fig. 2. Weight density (in g/cm$^3$) of Mo–Si–B alloys with Ti or Cr substitution (dotted line is the density of pure Ni = 8.9 g/cm$^3$).

were prepared by repetitive arc-melting of high-purity refractory metals, Si and B in an atmosphere of high-purity and oxygen gettered argon. These alloy compositions were selected from the BCC + $T_2$ + $Mo_3Si$ three-phase field in Mo–Si–B system. As indicated by the compositions, the molybdenum content in the alloys was systematically substituted by titanium. Alloys were subsequently annealed under an oxygen gettered argon environment at temperatures up to 1500 °C and for varying times up to 100 h. Oxidation tests in air were performed at temperatures between 1000 and 1400 °C. Back-scattered SEM (BSE) and powder X-ray diffraction were used to identify phases present in the cast as well as the annealed alloys.

The analysis of the structural stability of the silicide and borosilicide phases is based on the interatomic distances within the crystal structures. The electronic structure (density of states) at the ground states was also calculated as a guide to evaluate the relative phase stability. The energy band calculations for this purpose are based on the local-density approximation (LDA) to electronic exchange-correlation effects [5]. The calculations were performed using two different linear muffin–tin orbital (LMTO) programs for a comparison purpose: (1) a fast but not highly accurate tight-binding LMASA-47 code [6–9] and (2) a accurate full-potential LMART package [10,11]. The LMASA-47 code utilizes a self-consistent tight-binding linear muffin–tin orbital (TB-LMTO) method in the atomic sphere approximation (ASA) [6–8]. The LMART package utilizes the full-potential LMTO method (i.e without any atomic shape approximation). The crystal structure data including the internal atomic positions not restricted by the space group and the lattice parameters were taken from the reported the experimental results of crystal refinement work on single-phase $T_2$ powders [12,13]. Eigenvalues were calculated over 4500 *k*-points that represent the reciprocal lattice vectors from the irreducible part of the Brillouin zone. The criteria for the self-consistency were based on the total energy difference from the last iteration to the previous one not to exceed $10^{-6}$ Ry (which is equivalent to $2.18 \times 10^{-24}$ J). From the calculated electronic structures, the energy level is determined where the occupancy of bonding states are completely filled (typically signified by the presence of a minimum gap) and the critical number of total valence electrons that correspond to that energy position is estimated.

## 3. Results and discussion

### 3.1. High-temperature multi-phase microstructures

Examinations of the cast microstructures of the alloys showed the changes in the phase constituents associated with increased Ti substitution. An increase in the Ti substitution to Mo–20SiB–10Si results in the transformation of the two-phase $T_2$ + A15 alloys to the three-phase alloys of the BCC (MoTi) + $T_2$ + $Ti_5Si_3$ ($D8_8$) phases as shown in Fig. 3. The constituent phases in the cast alloys are retained following the high-temperature annealing (as exemplified in Fig. 4) indicative of the excellent thermal stability of the BCC + $D8_8$ + $T_2$ phase mixture.

The observed change in microstructures and high-temperature phase equilibrium with Ti addition can be understood from the fact that there is a limited solubility of Ti in the A15 phase in contrast to the $T_2$ and BCC phases. Further addition of titanium results in the formation of new phase equilibria involving the 5–3 silicides with two different prototypes; the $D8_8$ phase ($Ti_5Si_3$ prototype) and $T_1$ phase $(Mo,Ti)_5Si_3$($W_5Si_3$ prototype) as shown in Fig. 3(c). With a sufficient amount of Ti substitution for Mo, the two-phase field of A15 + BCC is replaced by the two-phase field of BCC + $D8_8$. In the Mo–Ti–Si–B system, the BCC + $D8_8$ two-phase field and the $T_2$ phase result in a stable three-phase field of BCC + $D8_8$ + $T_2$ as depicted in Fig. 3(d).

Fig. 4 shows an SEM micrograph of Mo–40Ti–20Si–10B and Mo–50Ti–20Si–10B after a 1400 °C heat treatment up to 100 h confirming the thermal stability of the Ti-rich BCC + $D8_8$ + $T_2$ three-phase field. In fact, the three-phase microstructures can be extended at least up to 80% substitution of Ti for Mo as shown in the Mo-60Ti-20Si-10B as-cast alloys (Fig. 5(a) and (b)). The XRD observation (Fig. 5(c)) verifies the major presence of the three phases in the Ti-rich Mo–Ti–Si–B alloys. Recently, a new compound of $Ti_6Si_2B$ (a hexagonal 6-2-1 phase – space group $P6_3/mcm$) has been observed in the Ti–Si–B alloys forming a ternary eutectic with the BCC and $D8_8$ phases in the as-cast microstructures [13,14]. A further study is needed to identify the phase relation between the 6-2-1 phase with the $T_2$ phase. The absence of the 6-2-1 phase in (Ti-rich) Mo–Ti–Si–B alloys (Fig. 5) suggests a much more limited (Mo,Ti) solid solution (<15%) at its metal sites within the quaternary Mo–Ti–Si–B system. The EDS measurements on the Ti-rich Mo–Ti–Si–B alloys also

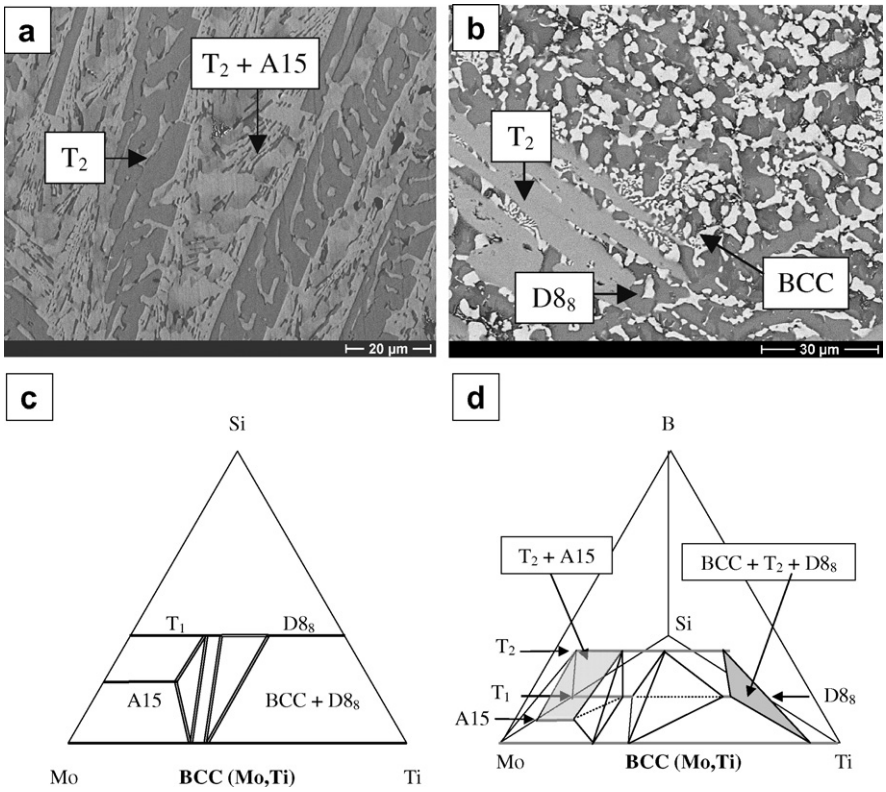


Fig. 3. Back-scattered SEM micrograph of multi-phase microstructures in: (a) two-phase (A15 + $T_2$) Mo–20Ti–20Si–10B and (b) three-phase (BCC + $T_2$ + $D8_8$) Mo–35Ti–20Si–10B cast alloys. The change in the phase equilibrium: A15 ⇒ BCC + $D8_8$ with a sufficient Ti substitution for Mo in the Mo–Ti–Si system as depicted in (c) consequently yields: A15 + $T_2$ ⇒ BCC + $D8_8$ + $T_2$ three-phase field in the Mo–Ti–Si–B quaternary system shown in (d). Some of the phase constituents are removed to clarify the view on the three-phase field.

showed that the $Ti_5Si_3$ ($D8_8$) phase has a similarly low Mo substitution for Ti (<10%).

### 3.2. Phase stability analysis

The stability of the new three-phase equilibrium can be attributed not only to the high melting (Mo–Ti) BCC and Ti-rich $D8_8$ phases, but also to the retention of the heavily Ti-alloyed $T_2$ phase. In part, this can be explained by the strong similarity of the alloying behavior in the $T_2$ phase to that of BCC phase and the favorable electronic factor associated with it [15]. It has been shown that due to the presence of BCC-like clusters and the strong Mo–Mo directional bonding embedded within the $T_2$ phase, there is an extended alloying between Mo with a wide range of transition metals such as Ti [15]. In contrast, as the current work demonstrates, the $D8_8$ phase and the 6-2-1 phases appear to show a more limited extension of Mo substitution for Ti. The differences in the alloying behavior can be traced to the geometric and electronic factors (i.e the valence electron numbers) that contribute to the structural stability of the three phases.

Analysis of the interatomic distances and electronic structure has been performed to further compare the relative stability of the three phases (6-2-1, $D8_8$ and $T_2$) and is summarized in Table 1. A number of observations can be made on the roles of these factors to the stability of the three phases. First, both $Mo_5SiB_2$ ($T_2$) and $Ti_5Si_3$ ($D8_8$) phases have a high melting temperatures exceeding 2000 °C, whereas the 6-2-1 phase has a surprisingly much lower melting temperature (below 1400 °C [13]). Secondly, from the interatomic distances within the crystal structures in Table 1, it can be inferred that the high thermal stability of the $D8_8$ phase is rooted in the strong Ti–Si (covalent) bonds in addition to the Ti–Ti interactions. As shown in the table, there is a relatively large contraction in the interatomic distance of Ti–Si atoms and Ti–Ti atoms in the $D8_8$ phase (relative to the Ti–Ti interatomic distance in the HCP structure). This is consistent with the analysis of the cohesive stability of

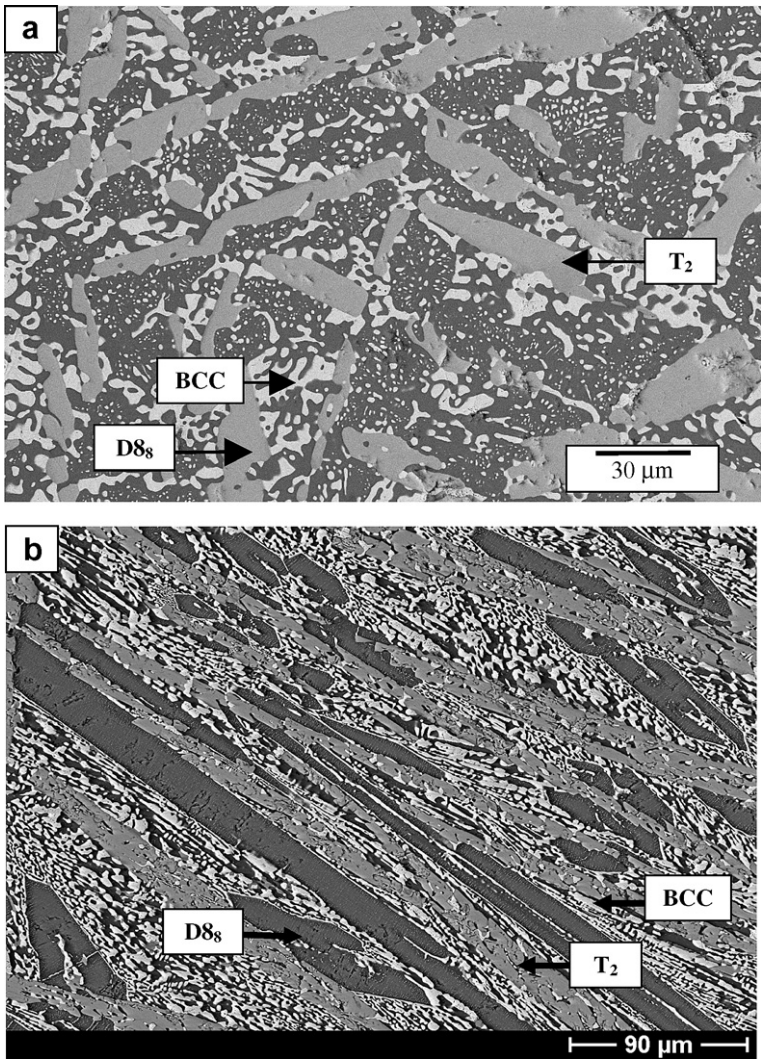


Fig. 4. BSE micrograph of: (a) Mo–40Ti–20Si–10B and (b) Mo–50Ti–20Si–10B after 1400 °C annealing for 24 h showing the three-phase BCC + $D8_8$ + $T_2$ microstructures. Longer annealing time (up to 100 h) shows the presence of the same constituent phases.

the $Ti_5Si_3$ which is attributed to the presence of strong bonding of Ti–Si and Ti–Ti atoms [16]. The stability of $T_2$ phase relies also on the metal–metalloid contacts as evidenced by the contraction of Mo–Si and Mo–B interatomic distances (to a lesser degree than that of $Ti_5Si_3$ phase). The difference however is in the interatomic distance of Mo–Mo atoms which shows an almost similar value to that of Mo–Mo atoms in the BCC phase. In fact, further analysis on the structure has shown the presence of 'mini-BCC' networks within the structure which enables a strong cohesive stability similar to that of the BCC structure [5]. This is unique in that typically with intermediate phase type of metal–metalloid phases, the metal–metal contacts (i.e similar to the structure of the elemental metals) will *compete* with the metal–metalloid contacts for the most stable structure. The $T_2$ phase enables metal–metal (in a BCC-like atomic environment) contacts to *complement* the metal–metalloid contacts (surrounding the BCC-like clusters). The 6-2-1 crystal structure is somewhat similar to that of $T_2$ phase where both the metal–metal (i.e. Ti–Ti contacts) and metal–metalloid contacts play important roles to the stability of the structure. The difference however is that the Ti–Ti contacts exert a much weaker directional bonding due to the lower concentration of d-electrons in comparison to that of BCC-like environment such as the Mo–Mo clusters within the $T_2$ phase [5]. In fact, the relatively low thermal

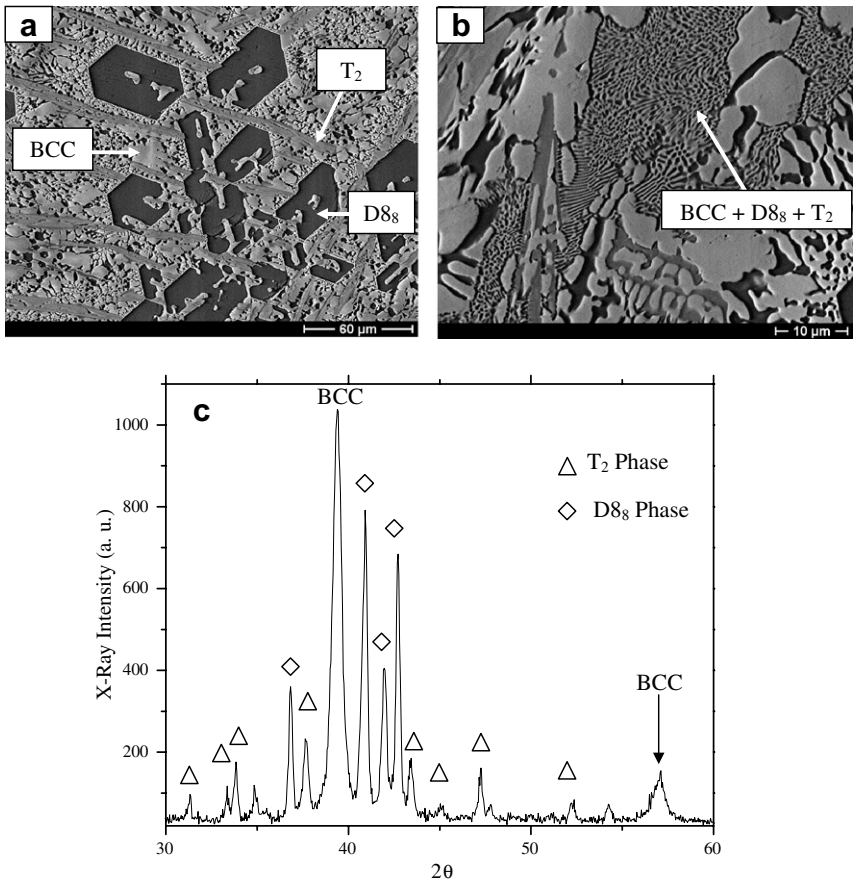


Fig. 5. (a) and (b) Mo–60Ti–20Si–10B as-cast alloys composed of BCC + $D8_8$ + $T_2$ phases. The XRD traces in (c) confirm the SEM observation. The Ti-rich $T_2$ crystal structure refinement yields the lattice parameter of $a = 0.6079$ nm, $c = 1.1462$ nm. Minor amount of TiB may also be present.

Table 1
Stability analysis on the $T_2$ and $D8_8$ and 6-2-1, phases

| Phases | Melting temperature (°C) | Percentage of contraction in the shortest atomic contacts (%) | Total number of valence electrons (VE) | Total number of VE at the DOS min. position | ΔVE |
|---|---|---|---|---|---|
| $Ti_6Si_2B$ | 1395 | Ti–Ti: 1.8<br>Ti–Si: 4.9<br>Ti–B: 8 | 35 | 36.5 | +1.5 |
| $Ti_5Si_3$ ($D8_8$) | 2130 | Ti–Ti: 12.4<br>Ti–Si: 6.1 | 32 | 32.5 | +1.5 |
| $Mo_5SiB_2$ ($T_2$) | 2100[a] | Mo–Mo: 1.09<br>Mo–Si: 5.8<br>Mo–B: 2.6 | 40 | 36 | −4.0 |

[a] Incongruent melting at the $T_2$ stoichiometric composition due to the peritectic reaction of MoB + L ⇒ $Mo_5SiB_2$ [14].

stability of the Ti-rich 6-2-1 represents a classical example of the underlying physical principle in the phase stability in transition metal (TM)–metalloid intermediate phases as proposed by Gelatt et. al [16]. With the 'insertion' of metalloid elements (B and Si) into a transition metal-rich (Ti) compound, there are two competing factors; (1) the strong hybridization between the transition metal d states and the s–p states on the metalloids and (2) the weakening of the bonding between transition metal

atoms by the departure of the TM–TM interatomic distance from the 'normal' interatomic distance in the pure transition metal to accommodate the metalloids within the compound. In the case of the $T_2$ phase, the Mo–Mo contacts 'preserved' in the mini-BCC network are almost undisturbed by the presence of Mo–metalloid contacts and hence it retains a high cohesive stability. On the other hand, in the case of the 6-2-1 phase, such cluster symmetry is non existent. As a result, the melting temperature is much lower than that of $T_2$ phase. This is not the case for the $D8_8$ phase since there are strong contractions of Ti–Ti atomic metal contacts in addition to the hybridization of the Ti d states and s–p states of Si and B.

Examination of the electronic structure of the $Ti_6Si_2B$ indeed confirms the analysis of the interatomic distances and may explain the limited solubility in the $D8_8$ and the 6-2-1 phases based on the observations of the optimum valence electron numbers for the cohesive stability of these compounds. It has been established previously that a thorough separation between bonding and anti-bonding regions in the electronic structure of a metal–metalloid compound is characteristic of covalency and high cohesive stability. A critical valence electron (VE) number would therefore refer to the value of total number of valence electron that favors the complete filling of the bonding states [17]. A critical VE number (per compound) would therefore bring the highest occupied states (Fermi energy level) of the crystal structure to the position that separates the bonding and anti-bonding states. A low density of states at the Fermi level is favorable for the phase stability. For example, the stability of the BCC phase is favorable with the valence electron number (VE) between 5 and 6 with the optimal VE number of 5.5 corresponding to the maximum cohesive energy [17]. The VE number of 5.5 corresponds to the position of the minimum gap in the density of states (DOS) of the BCC phase. For a full phase stability analysis, the role of the vibrational and configurational entropies must also be taken into account which was not included in these factors. However, as has been shown in a wide variety of transition metal based intermetallics such as silicides, carbides and aluminides [18–21], the most stable and highest melting crystal structures tend to exhibit a minimum gap in their total DOS and that the position of the Fermi energy level (which constitutes the highest occupied energy states at the ground state) is very close to the minimum gap. This trend seems to favor alloying additions that facilitate the minimum gap position. Following this line of reasoning, an analysis of the position of the minimum gap within the total DOS has been performed for the $T_2$ phase.

Fig. 6 shows the calculated DOS for the three intermetallic phases and Table 1 summarizes the observed optimal VE numbers of the three compounds along with their respective VE numbers. The DOS for all phases shows the presence of minimum gap near the Fermi level and as indicated previously it is due to the presence of both metal–metal atomic or metal–metalloid directional bonding. The DOS contribution of the metal–metal bonding is dominant near the Fermi energy level as shown in the partial DOS of metal d-bands (as represented in the shaded light-grey area in Fig. 6). On the other hand, the DOS contribution of the metal–metalloid contacts (mostly of p-bands) is positioned at a much lower energy (dark-grey area). This is consistent with the fact that in these three (metal-rich) phases, the metal–metal contacts are most dominant. However, there is a difference in terms of the relative energy positions (on the $x$-axis) that corresponds to the critical valence electron number (marked by the arrow position in Fig. 6) to the Fermi energy level (zero position). By integrating the DOS area between the two energy positions, the critical valence electron numbers (the integrated area difference) were estimated and tabulated in Table 1. For the $D8_8$ and 6-2-1 phases, the difference between the critical valence electron (VE) numbers to the compound valence electron number is only +1.5 VE per compound. This is in contrast with the $T_2$ phase where there is a greater difference in the VE numbers between the critical VE number and VE numbers of the compound (4 VE per compound). Thus, there is a greater tendency to alloy Mo with transition metals that will reduce the overall VE. Therefore, transition metals with lower VE numbers such as Nb or Ti will be favorable. Comparatively, both $D8_8$ and 6-2-1 phases have a much lesser tendency to alloy Ti with Mo since the VE number for these compounds are only 1.5 VE below the critical number.

### 3.3. Oxide layer structures

The cross-section microstructures of the oxide layers on the surface after oxidation tests in air at 1100 °C for 10 h and 1400 °C for 24 h respectively are shown in Figs. 7 and 8. The oxide layer sequence in the Mo–Si–B alloys is composed of borosilica at

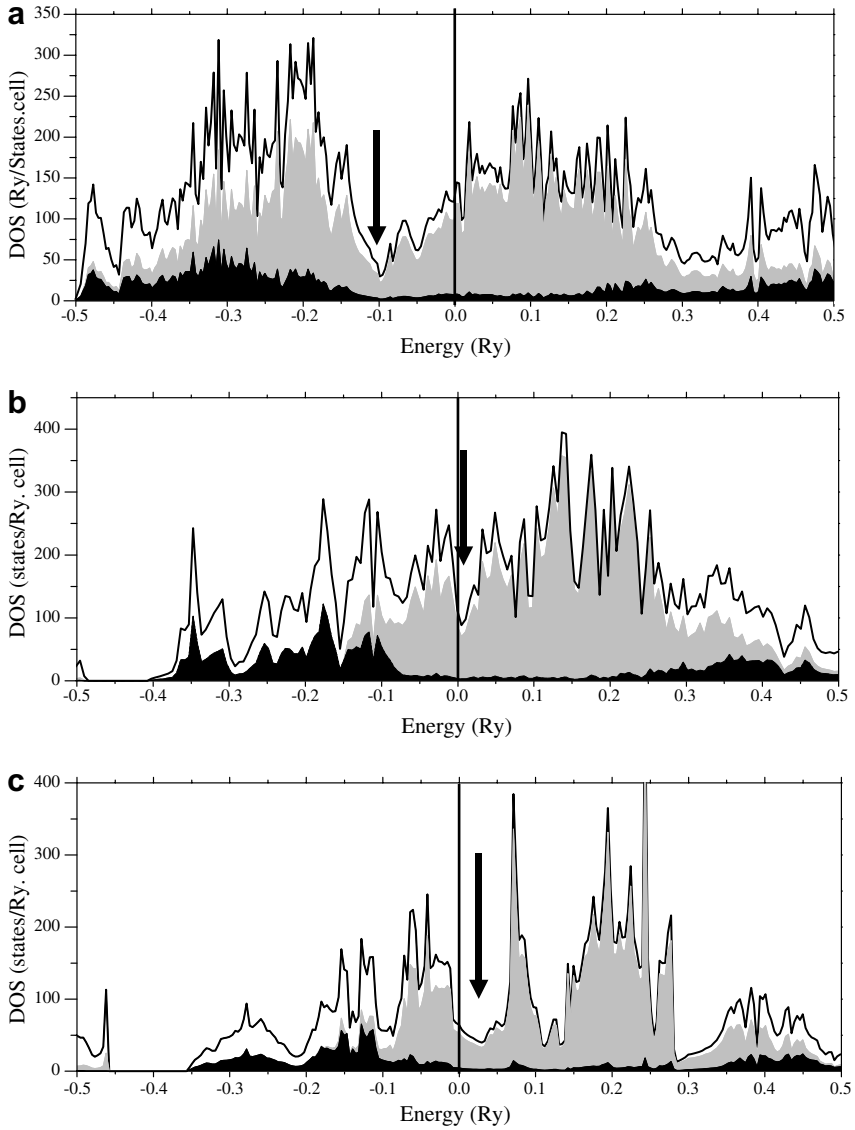


Fig. 6. The total and partial density of states of: (a) $Mo_5SiB_2$ ($T_2$), (b) $Ti_5Si_3$ ($D8_8$) and (c) $Ti_6Si_2B$ phases showing a visible presence of a DOS minimum gap position (arrow). The total and partial DOS are plotted relative to the Fermi energy level (solid vertical line) which corresponds to the highest occupied states within the crystal structure at the ground state at 0 K. The $x$-axis spans $\pm$ 0.5 Ry from the Fermi level. The dark area represents the partial DOS from the p-bands of the metalloid atoms whereas the light-grey area represents the contribution from the d-bands of the respective metal atoms. In all cases, the d–d metal interactions dominate the DOS near the Fermi level. For the BCC and $T_2$ phases, the position for the optimum VE numbers is well *below* the Fermi level whereas for each of the $D8_8$ and 6-2-1 phases, the position is slightly *above* the Fermi level.

the outermost surface followed by the $MoO_2$ layer and the BCC + borosilica layers. As shown previously [22], the sequence is a consequence of the limited diffusion of oxygen into the substrate primarily due to the formation of the borosilica as an effective oxygen barrier layer.

The layer structures change with the Ti addition in a significant way as noted in Figs. 7 and 8. The most important changes relate to the formation of a crystalline layer at the outermost surface with increasing Ti substitution for Mo. With a small addition of the Ti, there is the development of crystalline oxides within the borosilica glass; particularly near the surface. Previous study of the oxidation resistance of (Ti,Mo)$Si_2$ [23] suggested that there is a concurrent formation of crystalline

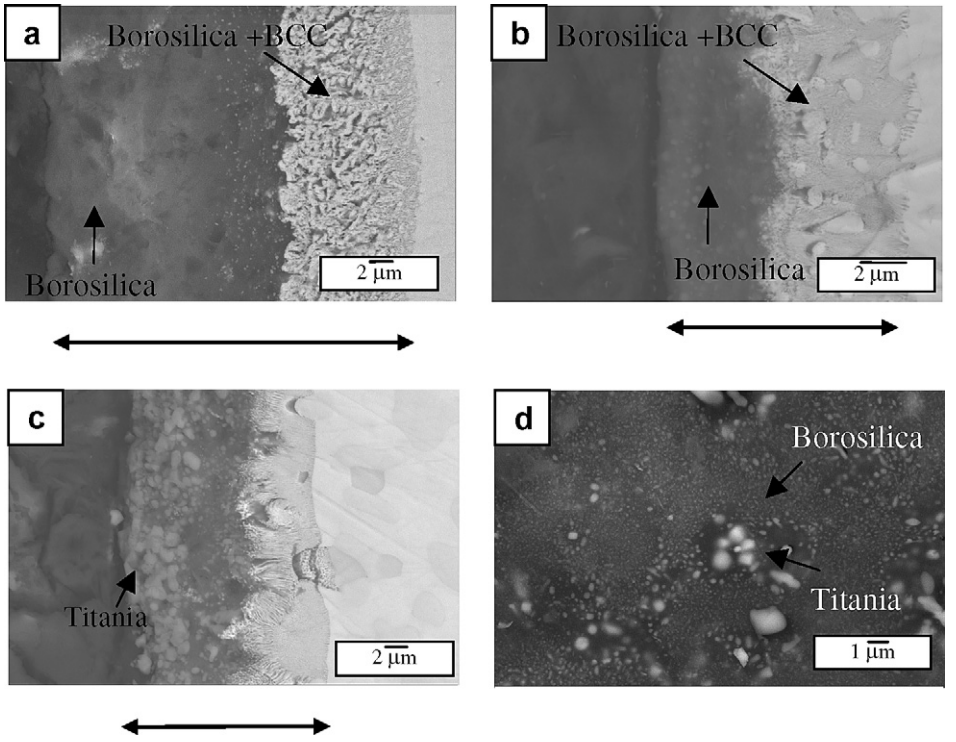


Fig. 7. Back-scattered SEM images of cross-sectioned microstructures in (a) Mo–20Si–10B, (b) Mo–5Ti–20Si–10B and (c) Mo–20Ti–20Si–10B alloys after an oxidation test of 1100 °C for 10 h. The oxide structures in the Mo–Si–B alloys are composed of the borosilicate outer layer and the inner layer of the borosilicate + BCC mixtures a shown in (a). With a small substitution of Ti for Mo (such as 5 at.%), a thinner borosilicate oxide layer develops wherein mostly titania particles were observed as shown in the plain-viewed SEM image in (d). With a higher Ti substitution (e.g. in c), continuous $TiO_2$ layer starts to form above the borosilicate layer. The arrows mark the oxide scale.

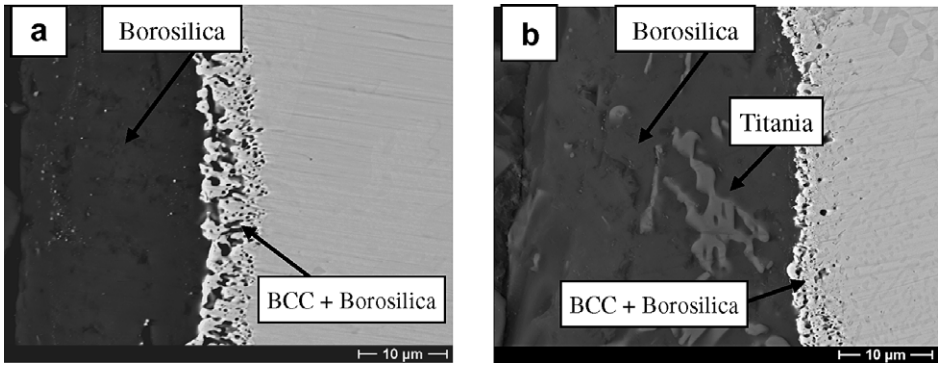


Fig. 8. Cross-sectioned SEM microstructure images of: (a) Mo–20Si–10B and (b) Mo–5Ti–20Si–10B after exposure in air at 1400 °C for 24 h.

titania and silica. With the titanium substitution in $MoSi_2$, it was reported that there was an increase in oxidation resistance initially due to the low O diffusion in the crystalline silica, but with an increased level of Ti substitution, there was an increase in the oxidation rate. In the current study, the oxide layer thickness of the Ti-substituted alloys remains relatively thin to at least 1100 °C. This is consistent with the recent oxidation study on Ti–Si–B alloys which showed that the outermost oxide scale is mostly titania after exposure at 1100 °C in air [24].

From the 1100 °C tests, the oxide layer thickness of Ti-substituted Mo–Si–B alloys (~25 μm) is quite

comparable in size scale with that of the Mo–Si–B alloys (~20 μm) as depicted in Fig. 8. The layer structures are composed of a mixed titania + borosilica near surface and mostly borosilica underneath. The difference in the oxidation resistance may be rooted in the stability of the titania + borosilica mixtures as an oxidation barrier. Additional quantitative oxidation studies for more extended periods are in progress to examine the promising oxidation resistance.

## 4. Summary

There is an extended solubility of Ti to substitute for Mo in Mo–Si–B alloys due to the large solubility of Ti in $Mo_5SiB_2$ ($T_2$) and the Mo solid solution (BCC) phases. A stable high-temperature three-phase mixture of BCC + $D8_8$ + $T_2$ can be extended into the Ti-rich side of the Mo–Ti–Si–B system. The substitution of Mo by Ti allows for the formation of oxidation resistant Mo–Ti–Si–B alloys with a significantly reduced weight density.

## Acknowledgements

The support of AFOSR (FA9550-06-1-023333) and ONR (N00014-02-1-0004) are gratefully acknowledged.

## References

[1] J.H. Perepezko, C.A. Nunes, S.H. Yi, D.J. Thoma, in: C.C. Koch, C.T. Liu, N.S. Stoloff, A. Wanner (Eds.), High Temperature Ordered Intermetallic Alloys VII, MRS, Pittsburgh, PA, 1997, p. 1.
[2] J.H. Perepezko, R. Sakidja, S. Kim, in: J.H. Schneibel et al. (Eds.), High Temperature Ordered Intermetallic Alloys IX, MRS, Pittsburgh, PA, 2001, p. N4.5.1.
[3] R. Sakidja, H. Sieber, J.H. Perepezko, in: A. Crowson, E.S. Chen, J.A. Shield, P.R. Subramanian (Eds.), Molybdenum and Molybdenum Alloys, TMS, Warrendale, PA, 1998, p. 99.
[4] J.H. Schneibel, C.T. Liu, D.S. Easton, C.A. Carmichael, Mater. Sci. Eng. A 1&2 (1999) 78.
[5] S.H. Vosko, L. Wilk, M. Nusair, Can. J. Phys. 58 (1980) 1200.
[6] O.K. Andersen, Phys. Rev. B 12 (1975) 3060.
[7] O.K. Andersen, O. Jepsen, Phys. Rev. Lett. 53 (1984) 2571.
[8] O.K. Andersen, Z. Pawlowska, O. Jepsen, Phys. Rev. B 34 (1986) 5253.
[9] http://www.fkf.mpg.de/andersen/.
[10] S.Y. Savrasov, Phys. Rev. B 54 (1996) 16470.
[11] S.Y. Savrasov, 2004. <http://physics.njit.edu/~savrasov/>.
[12] C.J. Rawn, J.H. Schneibel, C.M. Hoffmann, C.R. Hubbard, Intermetallics 9 (2001) 209.
[13] A.S. Ramos, C.A. Nunes, G. Rodrigues, P.A. Suzuki, G.C. Coelho, A. Grytsiv, P. Rogl, Intermetallics 12 (2004) 487.
[14] Y. Yang, Y.A. Chang, L. Tan, Intermetalllics 13 (2005) 1110.
[15] R. Sakidja, J.H. Peperezko, Metal. Mater. Trans. A 3 (2005).
[16] C.D. Gelatt, A.R. Williams, V.L. Maruzzi, Phys. Rev. B 27 (1983) 2005.
[17] D.G. Pettifor, J. Phys. F 7 (1977) 613.
[18] C.L. Fu, A.J. Freeman, T. Oguchi, Phys. Rev. Lett. 54 (25) (1985) 2700.
[19] S. Ohnishi, A.J. Freeman, M. Weinert, Phys. Rev. B 28 (1983) 6741.
[20] J.-H. Xu, T. Oguchi, A.J. Freeman, Phys. Rev. B 35 (1987) 6940.
[21] J. Xu, A.J. Freeman, Phys. Rev. B 40 (11) (1989) 11927.
[22] J.S. Park, R. Sakidja, J.H. Perepezko, Scripta Mater. 46 (11) (2002) 759.
[23] J. Schlichting, Ceramurgia Int. 4 (4) (1978) 162.
[24] E.C.T. Ramos, G. Silva, A.S. Ramos, C.A. Nunes, C. Baptista, Mater. Sci. Eng. A 363 (2003) 297.